PCCP

Cite this: *Phys. Chem. Chem. Phys.*, 2011, **13**, 15644–15656

www.rsc.org/pccp

PAPER

Infrared spectra of the protonated neurotransmitter histamine: competition between imidazolium and ammonium isomers in the gas phase†

Anita Lagutschenkov,[a] Judith Langer,[a] Giel Berden,[b] Jos Oomens[bc] and Otto Dopfer*[a]

Received 24th May 2011, Accepted 11th July 2011
DOI: 10.1039/c1cp21681c

The infrared (IR) spectrum of protonated histamine (histamineH^+) was recorded in the 575–1900 cm^{-1} fingerprint range by means of IR multiple photon dissociation (IRMPD) spectroscopy. The IRMPD spectrum of mass-selected histamineH^+ ions was obtained in a Fourier transform ion cyclotron resonance mass spectrometer coupled to an electrospray ionization source and an IR free electron laser. A variety of isomers were identified and characterized by quantum chemical calculations at the B3LYP and MP2 levels of theory using the cc-pVDZ basis set. The low-energy isomers are derived from various favourable protonation sites—all of which are N atoms—and different orientations of the ethylamine side chain with respect to the heterocyclic imidazole ring. The measured IRMPD spectrum was monitored in the NH_3 loss channel and exhibits 14 bands in the investigated spectral range, which were assigned to vibrational transitions of the most stable isomer, denoted **A**. This imidazolium-type isomer **A** with protonation at the imidazole ring and *gauche* conformation of the ethylamine side chain is significantly stabilized by an intramolecular ionic Nπ–H^+···Nα hydrogen bond to the ethylamino group. The slightly less stable ammonium-type isomer **B** with protonation at the ethylamino group is only a few kJ mol^{-1} higher in energy and may also provide a minor contribution to the observed IRMPD spectrum. Isomer **B** is derived from **A** by simple proton transfer from imidazole to the ethylamino group along the intramolecular Nπ–H^+···Nα hydrogen bond *via* a low barrier, which is calculated to be of the order of 5–15 kJ mol^{-1}. Significantly, the most stable structure of isolated histamineH^+ differs from that in the condensed phase by both the protonation site and the conformation of the side chain, emphasizing the important effects of solvation on the structure and function of this neurotransmitter. The effects of protonation on the geometric and electronic structure of histamine are evaluated by comparing the calculated properties of isomer **A** with those of the most stable structure of neutral histamine **A(n)**.

1. Introduction

2-(1H-imidazol-4-yl)ethanamine, also known as histamine ($C_5N_3H_9$, Fig. 1), is a biogenic monoamine and belongs to the family of fundamental neurotransmitters.[1–3] Histamine occurs in animal organisms and plant tissues,[4] and is synthesized in basophils and mast cells from histidine through one-step enzymatic decarboxylation. Histamine is of importance in the immune response to foreign pathogens and involved in allergic reactions. In this context, histamine triggers the inflammatory response by dilating the blood vessels, which results in an enhanced permeability of the vessels and thus in increased fluid content in the cells. Thus, skin swelling occurs as a symptom of an allergic reaction. Furthermore, histamine interacts with at least four receptors, denoted H_{1-4}, with different resulting biological activities. For example, the interaction with

[a] *Institut für Optik und Atomare Physik, Technische Universität Berlin, Hardenbergstraße 36, 10623 Berlin, Germany. E-mail: dopfer@physik.tu-berlin.de; Fax: +49 30-31423018; Tel: +49 30-31423017*
[b] *FOM Institute for Plasma Physics Rijnhuizen, Edisonbaan 14, 3439 MN Nieuwegein, The Netherlands*
[c] *van't Hoff Institute for Molecular Sciences, University of Amsterdam, Science Park 904, 1098 XH Amsterdam, The Netherlands*

† Electronic supplementary information (ESI) available: Geometries, energies, charge distributions, fragment ion structures and additional vibrational properties of various histamine and histamineH^+ isomers. See DOI: 10.1039/c1cp21681c

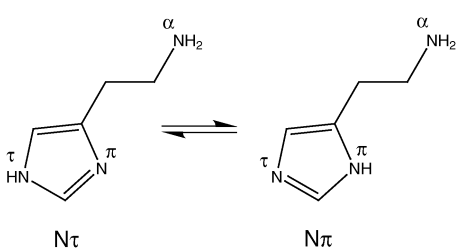

Fig. 1 Tautomeric structures Nτ and Nπ of neutral histamine.

the H_2 receptor invokes gastric secretion, which is expected to produce gastric ulceration.[5–8] As histamine occurs under physiological conditions (pH = 7.4) predominantly in its singly protonated form (>96%),[5,9] characterization of isolated histamineH^+ and its interaction with the environment are required to understand these biophysical processes at the molecular level.

Owing to the two nitrogen atoms of the imidazole unit, histamine exists in two tautomeric forms (Fig. 1), denoted Nπ–H and Nτ–H (or N1–H and N3–H). Histamine offers two basic N atoms for protonation, one at the imidazole ring (Nτ/π) and one at the terminal amino group of the aliphatic side chain (Nα). Protonation at Nτ/π generates an imidazolium ion, whereas protonation at Nα produces an ammonium ion. Under physiological conditions, the excess proton is located at Nα due to its higher pK_a value of ~9.4 as compared to Nτ/π with pK_a ≈ 5.8.[9] In addition, as a result of the flexibility of the ethylamine side chain (Fig. 2), histamine(H^+) can adopt folded *gauche* and extended *trans* structures, yielding a variety of possible conformeric tautomers. A particular feature of histamine(H^+) involves the possibility of several *gauche* isomers to form intramolecular N–$H^{(+)}$···N hydrogen bonds, which lead to additional stabilization with respect to the corresponding *trans* isomers in the gas phase. In solution, however, the energy gain through solvation competes with the stabilization through these intramolecular hydrogen bonds. There might be further intramolecular interactions, like cation–π interactions between the protonated side chain and the aromaticπ-electron system of imidazole.[10–13] For a deeper understanding of all these interactions and the resulting structure–function relationship of this fundamental neurotransmitter at the molecular level, it is essential to evaluate the effects of the environment and the charge state on the structural and energetic properties.

Previous experimental studies of histamine(H^+) reveal that the tautomeric and conformational structure and the protonation site observed strongly depend on its charge state and the environment. Early X-ray crystallographic studies on ionic histamine*HBr salts yield an ammonium-type Nτ-tautomeric histamineH^+ ion with the protonated ethylamine side chain in *trans* conformation.[14] Subsequent vibrational analysis of infrared (IR) and Raman spectra of the related histamine*HCl salt is consistent with this result.[15] Interestingly, X-ray studies of crystals of neutral histamine grown from dry benzene solutions reveal a Nπ-tautomeric form in *trans* conformation, with no evidence for contributions from a Nτ tautomer, illustrating the large impact of protonation and counter ions

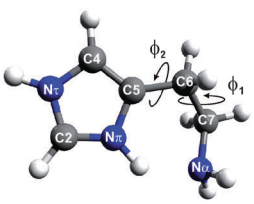

Fig. 2 Structure and atomic labels of isomer **A** of histamineH^+ ($C_5H_{10}N_3^+$) at the B3LYP/cc-pVDZ level. The dihedral angles ϕ_1 and ϕ_2 define the conformation of the various possible isomers of histamineH^+, while the position of the protons at Nπ, Nτ and Nα defines tautomeric isomers.

on the preferred structure of histamine.[16] In contrast to the crystalline phase, the structure of histamineH^+ in solution is more flexible and less well defined. NMR studies in aqueous solution[5,17] confirm that histamine occurs at pH ≈ 7.4 with >96% as an ammonium monocation of both the Nπ and Nτ tautomers, with the Nτ form being slightly preferred and regarded as the physiologically active species when interacting, *e.g.*, with the H_1 receptor.[5,9] However, at 37 °C the reported differences in free energy are less than 4 kJ mol^{-1}, so both tautomers may contribute substantially.[8] In addition, the population of *gauche* and *trans* conformations of histamineH^+ was estimated as 45 and 55% in aqueous solution, respectively.[5] The analyses of more recent IR and Raman spectra in conjunction with calculations at the B3PW91/6-31+G* level are consistent with respect to that the *trans* Nτ-tautomeric ammonium isomer is the predominant isomer in water.[18] Similar to the protonated species, early ^{13}C-NMR studies indicate the preference for the Nτ tautomer also for neutral histamine in aqueous solution.[19] More recent IR and Raman spectra of histamine in H_2O and D_2O as well as calculations based on a continuum solvent model confirm that the Nτ tautomer in *gauche* conformation is the most stable isomer of neutral histamine in aqueous solution.[20] However, as different calculations do not yield uniform results, the structure of neutral histamine in solution is still under debate.[20–25]

In order to eliminate the strong impact of the environment on the structure of histamine(H^+), experimental studies for these species isolated in the gas phase are required. However, such studies are scarce. Pioneering microwave experiments reveal the presence of one Nπ and three Nτ tautomers of neutral histamine in a molecular beam expansion.[26] Their structural identification was unambiguously confirmed by quantum chemical calculations.[26,27] In contrast to the condensed phase, all structures observed in the gas phase are *gauche* isomers. The most stable structure, denoted **A(n)**, is a *gauche* Nπ tautomer stabilized by an intramolecular Nπ–H···Nα hydrogen bond.[26,27] The only experimental data available for isolated histamineH^+ are derived from mass spectrometric experiments, which do however not provide any direct structural information.[28,29] No spectroscopic data are available for histamineH^+ in the gas phase. Thus, the current IR spectroscopic study provides the first experimental determination of the geometry of the protonated species free from interference with solvation effects. There are a large variety of quantum chemical studies, which investigate in some detail the structural, energetic and vibrational properties of isolated histamineH^+ isomers and the effects of solvation.[21,22,28,30–34] These calculations predict the *gauche* imidazolium ion (isomer **A**, Fig. 3) to be the most stable structure of the isolated molecule, followed closely in energy by the *gauche* ammonium-type Nτ tautomer (isomer **B**).[28,31]

There are two major strategies to IR spectroscopy of molecular ions and clusters in the gas phase, and their application to protonated aromatic ions (AH^+) has been reviewed recently.[35,36] The first technique involves single-photon dissociation of weakly bound cluster ions using table-top IR lasers based on difference frequency mixing or optical parametric oscillators.[37–39] This approach has initially been applied to protonated phenol[40–42] and benzene,[43,44] and since then to a large variety of other AH^+ ions.[45–50] This method can also be applied to weakly bound isolated AH^+ ions with low dissociation thresholds.[51–53]

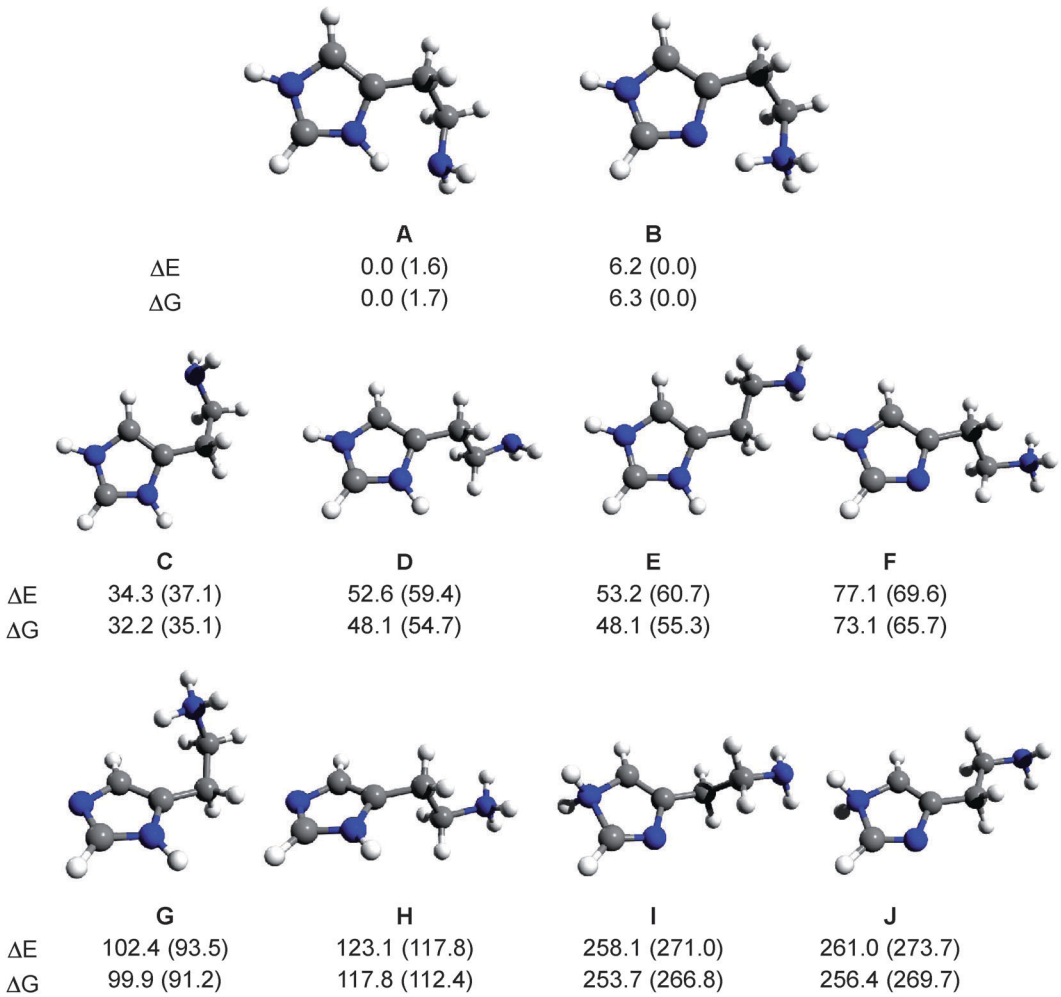

Fig. 3 Structures and relative energies (ΔE, top) and free energies (ΔG, bottom) of various isomers of histamineH^+ derived at the B3LYP/cc-pVDZ level. Corresponding MP2/cc-pVDZ values are given in parentheses. All energies are given in kJ mol^{-1}.

In an elegant approach,[54–56] a variety of simple protonated neurotransmitters were prepared by ionization-induced intracluster proton transfer occurring in a hydrogen-bonded phenol–neurotransmitter cluster. This approach produces a phenoxy-neurotransmitterH^+ dimer, the structure of which can subsequently be probed by IR photodissociation monitoring the loss of the phenoxy tag. Alternatively, the neurotransmitterH^+ can directly be generated upon post-ionization fragmentation and then probed by IR multiple photon dissociation (IRMPD). Owing to the complex photochemical production mechanism, the detected protonation site may however not necessarily be the energetically most favorable one of the isolated neurotransmitterH^+. In addition, this approach is limited to neurotransmitters and biomolecules, which can be transferred into the gas phase by thermal heating. The second major strategy involves IRMPD of strongly bound isolated ions using intense IR free electron lasers.[35,36,57–63] In the IRMPD process, the ion absorbs in a noncoherent fashion sequentially multiple IR photons until the lowest dissociation threshold is reached.[36] In recent years, IRMPD has successfully been coupled to electrospray ionization (ESI) sources to spectroscopically characterize AH^+ ions derived from larger biomolecules[36,64–67] and polycyclic aromatic hydrocarbon molecules,[68–71] as well as metal–organic complexes.[72–76] An elegant alternative route to unravel the protonation site and conformations of protonated biomolecules and their clusters involves IR hole-burning spectroscopy of ESI-generated ions in cryogenic ion traps.[77–79]

In a recent campaign, we recorded IRMPD spectra of a series of ESI-generated protonated neurotransmitters in the fingerprint range in a Fourier transform ion cyclotron resonance (FT-ICR) mass spectrometer, which was coupled to the IR beamline of the Free Electron Laser for Infrared eXperiments (FELIX). A thorough account of the results obtained for dopamineH^+ and serotoninH^+ has been given elsewhere.[12,13] The present work provides a detailed analysis of the IRMPD spectrum of histamineH^+ utilizing quantum chemical calculations at the B3LYP and MP2 levels of theory. The first spectroscopic data for this ion establish that the preferred protonation site of this fundamental neurotransmitter molecule in the gas phase is at the imidazole ring and not at the ethylamine side chain. In this respect, protonated histamine differs from all related neurotransmitterH^+ ions studied so far,[12,13,54–56] which exclusively prefer protonation at the alkylamino side chain.

2. Experimental and theoretical techniques

The IRMPD spectrum of mass-selected histamineH^+ ions was obtained in the 575–1900 cm^{-1} fingerprint range using the same strategy employed previously for related protonated neurotransmitters[12,13] and polycyclic aromatic hydrocarbon molecules.[68–70] Briefly, the IRMPD spectrum of histamineH^+ was recorded in a FT-ICR mass spectrometer coupled to the IR beamline of FELIX.[80,81] Histamine was purchased from Sigma-Aldrich (product number H7125) and used without further purification. HistamineH^+ ions were produced in an ESI source by spraying a $\sim 3 \times 10^{-5}$ molar solution of histamine dissolved in water/methanol (1 : 4) at a flow rate of ~ 10 μL min^{-1}. After accumulation and thermalization in a hexapole trap for 4 s, all ions were transferred into the ICR trap. Subsequently, histamineH^+ ions were mass selected and irradiated in the ICR trap for 3 s with IR laser radiation from FELIX operating at a repetition rate of 5 Hz. The macropulse energy varied between 65 and 31 mJ measured near 950 and 1685 cm^{-1}, respectively (see Fig. 4 for the detailed wavenumber dependence). The bandwidth of the FELIX radiation is specified as $\sim 0.5\%$ of the central wavelength, which corresponds to 5 cm^{-1} at $\nu = 1000$ cm^{-1}. The wavenumber step size varied between 3 and 8 cm^{-1}. Under the given experimental conditions, the only major fragmentation channel observed upon IRMPD of histamineH^+ ($m/z = 112$) was loss of NH_3 leading to fragment ions with $m/z = 95$. (A second higher-energy fragmentation channel yielding $m/z = 83$ is weaker than 10% of the $m/z = 95$ channel and thus neglected for further analysis, in particular because it exhibits the same IR action spectrum.) Parent and fragment ion intensities were monitored as a function of the laser frequency (Fig. 4), and the IRMPD yield shown in Fig. 5 was calculated as the integrated intensity ratio $I_{95}/(I_{95} + I_{112})$, which was linearly normalized for variations in the laser intensity displayed in Fig. 4. The IRMPD spectrum reveals 14 major bands labelled A–O in the spectral range investigated, and their positions, widths, and assignments are listed in Table 1. As expected, the depletion spectrum of the $m/z = 112$ parent ion is similar to the appearance spectrum of the $m/z = 95$ daughter ion. The depletion of the parent ion signal exceeds 20% at most intense resonances indicating

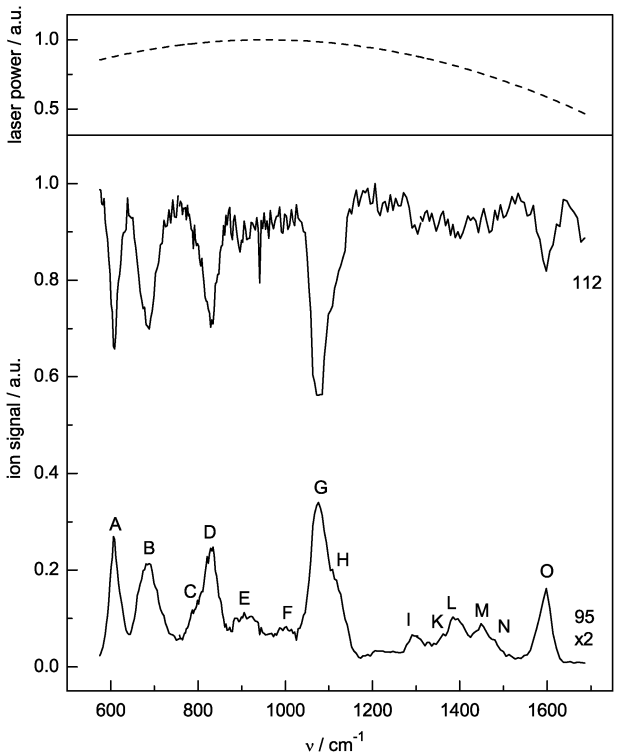

Fig. 4 Ion currents of histamineH^+ ($m/z = 112$) and the fragment channel with $m/z = 95$ (loss of NH_3) recorded in the fingerprint range (575–1680 cm^{-1}). The spectrum was actually scanned up to 1900 cm^{-1} but no transition was detected beyond 1600 cm^{-1} (band O). The variation in the IR laser intensity is given as dashed line. The positions and vibrational assignments of the bands A–O are listed in Table 1.

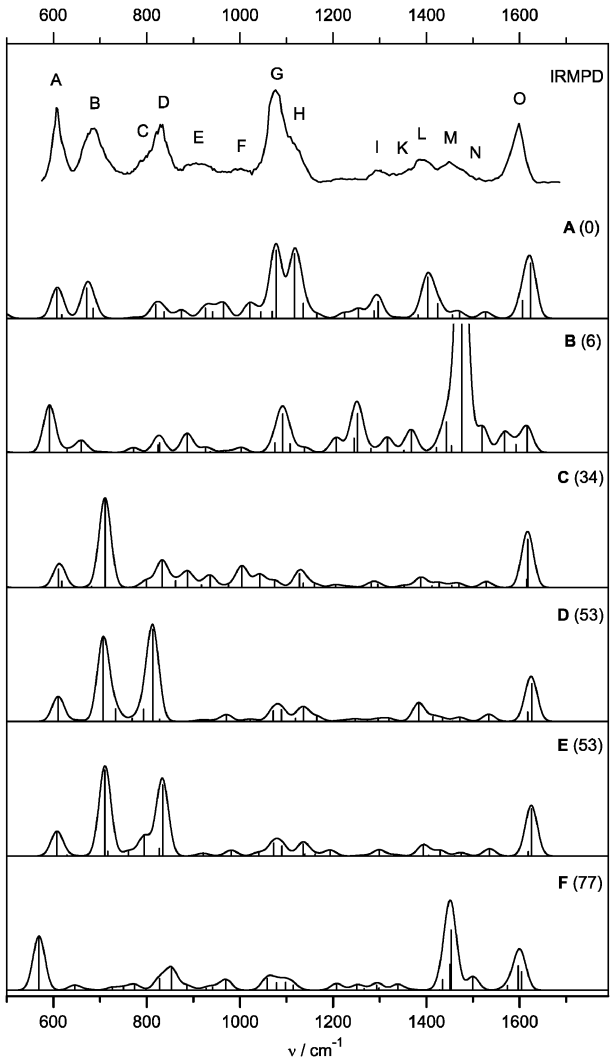

Fig. 5 IRMPD yield of histamineH^+ linearly normalized for IR laser intensity variations compared to linear IR absorptions spectra of the lowest-energy isomers **A–F** of histamineH^+ in energetic order (ΔE in kJ mol^{-1}) calculated at the B3LYP/cc-pVDZ level. The IR spectra are scaled by 0.98 and stick spectra are convoluted using FWHM = 30 cm^{-1}. The intensities of all calculated spectra are drawn on the same scale. The intensity of the intense transition of **B** is cut at $\sim 50\%$. The IR spectra calculated for the high-energy isomers **G–J** are available in Fig. S5 in ESI.†

Table 1 Experimental vibrational frequencies (in cm^{-1}) of histamineH^+ extracted from its IRMPD spectrum (Fig. 6) compared to frequencies of the isomers **A** and **A(n)** of protonated and neutral histamine calculated at the B3LYP/cc-pVDZ level

HistamineH^+[a], ν_{exp}	HistamineH^+ **A**[b], ν_{calc}	Histamine **A(n)**[b], ν_{calc}	Vibration[c]
1598 (34) O	1623 (95)	1577 (10)	ν_5(Im) = $\sigma_{CC}/\sigma_{CN}/\beta_{NH}/\beta_{CH}$
	1606 (30)	1605 (24)	β_{NH_2}(scissor)
1515 (—) N	1527 (12)	1474 (25)	ν_6(Im) = $\sigma_{CC}/\sigma_{CN}/\beta_{CH}/\beta_{CH}$
1453 (~60) M	1471 (10)	—	β_{NH}(Nτ) of excess H^+
	1456 (6)	1453 (3)	β_{CH_2}(scissor, C7)
	1425 (25)	1423 (10)	β_{CH_2}(scissor, C6)
1389 (58) L	1403 (71)	1403 (33)	ν_7(Im) = $\sigma_{CC}/\sigma_{CN}/\beta_{NH}/\beta_{CH}$
1359 (—) K	1382 (6)	1383 (10)	β_{CH_2}(wag, C7) and τ_{NH_2}
	1336 (2)	1335 (9)	β_{CH_2}(wag, C6) and β_{CH_2}(twist, C7)
1293 (35) I	1296 (29)	1359 (22)	$\sigma_{CC}/\sigma_{CN}/\beta_{CH}/\beta_{NH}$ and β_{CH_2}(wag, C6) and β_{CH_2}(twist, C7)
	1288 (13)	1288 (2)	β_{CH_2}(twist, C6) and β_{CH_2}(wag, C7) and τ_{NH_2}
	1255 (17)	1233 (2)	ν_{10}(Im) = σ_{CN}(sym) and β_{CH_2}(twist, C6) and β_{CH_2}(wag, C7)
	1224 (10)	1211 (5)	ν_8(Im) = σ_{CN} and β_{CH_2}(twist, C6) and β_{CH_2}(twist, C7)
	1165 (8)	1252 (12)	ν_9(Im) = β_{NH}/β_{CH}
	1136 (26)	1126 (3)	ν_{13}(Im) = σ_{CN} and β_{CH_2}(twist, C6) and τ_{NH_2}
1107 (~30) H	1117 (111)	1084 (64)	β_{NH}(Nπ) = ν_{12}(Im)
1075 (38) G	1078 (117)	758 (21)	ν_{21}(Im) = γ_{NH}(Nπ)
	1070 (12)	1116 (1)	ν_{11}(Im) = σ_{CN}(NτC4)/β_{CH}
	1045 (12)	1058 (10)	σ_{CC}(C6C7) and σ_{CN}(C7Nα)
997 (~55) F	1021 (26)	1009 (19)	σ_{CN}(C7Nα) and τ_{NH_2}
	965 (26)	994 (8)	ν_{14}(Im) = σ_{CN}(sym, Nπ)
	941 (11)	937 (31)	β_{CH_2}(twist, C6 and C7) and τ_{NH_2}
909 (~60) E	926 (18)	919 (18)	ν_{15}(Im) = σ_{CN}(sym, Nτ)
	875 (15)	881 (21)	σ_{CC}(C6C7)
	838 (12)	836 (34)	σ_{CC}(sym, C5C6 and C6C7) and β_{CH_2}(twist, C6)
830 (40) D	820 (24)	820 (25)	ν_{17}(Im) = γ_{CH} (in phase, C2 and C4)
788 (~35) C	778 (2)	787 (25)	ν_{16}(Im) = γ_{CH} (out of phase, C2 and C4)
	685 (17)	680 (7)	ν_{18}(Im) = $\gamma_{CN/CC}$
685 (53) B	671 (52)	—	γ_{NH}(Nτ) of excess H^+
	618 (6)	610 (7)	ν_{20}(Im) = $\gamma_{CN/CC}$
607 (23) A	607 (49)	652 (22)	ν_{19}(Im) = $\gamma_{CN/CC}$

[a] Peak positions and labels taken from the IRMPD spectrum in Fig. 6. The widths (FWHM) are given in parentheses. [b] IR intensities in km mol^{-1} are given in parentheses. Harmonic frequencies are scaled by 0.98. [c] The notation σ, γ, β, and τ refers to stretch, out-of-plane bend, in-plane bend, and torsional modes, respectively. ν_i(Im) denote corresponding normal modes of imidazole taken from ref. 97 and 98.

efficient IRMPD. As the IRMPD yield is normalized for parent ion fluctuations, it exhibits better signal-to-noise ratio than the depletion signal and will be compared to the calculated spectra. The width of the IRMPD bands of typically ~40 cm^{-1} arises from a variety of reasons. First, several overlapping vibrational transitions of a single isomer as well as signals from several isomers may contribute to the observed peaks resulting in spectral congestion. The finite laser bandwidth of ~0.5% (*i.e.*, 3–10 cm^{-1}) leads to additional broadening, along with an unresolved rotational fine structure of the ions at T = 300 K in the ICR cell. Rotational band contour simulations using the rotational constants of histamineH^+ (isomer **A**) calculated at the B3LYP/cc-pVDZ level (A = 4.72 GHz, B = 1.44 GHz, C = 1.15 GHz) suggest that up to 15 cm^{-1} of the observed width may be attributed to the unresolved rotational fine structure. Furthermore, the multiple photon absorption process itself results in heating of the ions during the long irradiation time which in turn leads to additional broadening.[36,82] The most narrow band at 607 cm^{-1} has a width of 23 cm^{-1}, which is close to the width expected from the rotational contour (15 cm^{-1}) and the laser resolution at this frequency (3 cm^{-1}). Despite its multiple photonic nature, the IRMPD spectrum predominantly reflects the absorption of the first IR photon (the reader is referred to ref. 36 for a recent review of the IRMPD mechanism) and thus justifies direct comparison with a calculated linear one-photon IR absorption spectrum.

Quantum chemical calculations at the B3LYP/cc-pVDZ and MP2/cc-pVDZ levels were performed for histamine(H^+) to identify various low-lying isomers on the potential energy surface and to evaluate their structural, energetic, and IR spectral properties.[83] Reported relative (free) energies ΔE and ΔG (298 K) include harmonic vibrational zero-point energy corrections scaled with a factor of 0.98 (B3LYP) and 0.97 (MP2).[12,13] If not stated otherwise, all coordinates were relaxed to locate stationary points on the potential energy surface. For all stationary points, frequency analysis ensured their nature as a minimum or transition state. Theoretical IR stick absorption spectra are convoluted with Gaussian line profiles using FWHM = 30 cm^{-1} to facilitate convenient comparison with the experimental IRMPD spectrum. A natural bond orbital (NBO) analysis was performed to evaluate charge distributions in histamine(H^+). For the two most stable histamineH^+ isomers, which are close in energy (**A** and **B**), higher levels of theory up to MP2/cc-pVQZ and CCSD(T)/cc-pVDZ were applied to ensure their energetic order.

3. Results and discussion

3.1 Vibrational and isomer assignment of IRMPD spectrum

Extended quantum chemical calculations were conducted at the B3LYP/cc-pVDZ and MP2/cc-pVDZ levels to establish the vibrational and isomer assignment of the transitions observed in the experimental IRMPD spectrum of histamineH^+. The structures and relative energies (ΔE and ΔG) of the most stable isomers labelled **A–J** resulting from a detailed search on the potential energy surface of the isolated ion are shown in Fig. 3. Only structures with protonation at one of the basic nitrogen atoms Nπ/τ/α were investigated. In agreement with previous calculations,[28,30,31] the three most stable isomers **A–C** are derived from *gauche* conformers of the neutral Nτ tautomer by protonation at either Nπ (**A**, **C**) or Nα (**B**). Thus, **A** and **C** are imidazolium ions, whereas **B** corresponds to an ammonium isomer. In all three isomers, the (protonated) amino group of the ethylamine side chain points toward the imidazole ring ($-90° < \phi_1 < 90°$, Fig. 2). The isomers **A** and **B** are similar in energy (to within 10 kJ mol^{-1}) and by far the most stable structures because they are both substantially stabilized by strong and short intramolecular N–H^+···N hydrogen bonds (R = 1.79 and 1.59 Å). Actually, both isomers can be interconverted into each other by simple proton transfer along the N–H^+···N hydrogen bond through a transition state with a low barrier calculated to be of the order of 5–15 kJ mol^{-1} (vide infra). Structure **C** is ~30–40 kJ mol^{-1} less stable than **A** and seems to slightly benefit from a weak and long CH···N contact (R = 2.45 Å). Two more *trans* conformers of imidazolium ions, denoted **D** and **E**, with the amino group of the ethylamine side chain pointing away from the imidazole unit ($\phi_1 > 90°$ or $\phi_1 < -90°$), are located ~50–60 kJ mol^{-1} above **A**. Isomer **F** is the lowest-energy *trans* ammonium isomer at $\Delta E \approx$ 70–80 kJ mol^{-1}. The two structures **G** and **H** are *gauche* and *trans* ammonium isomers with the imidazole proton at Nπ (rather than at Nτ) and $\Delta E \approx$ 90–100 kJ mol^{-1}. The isomers **I** and **J** with two protons at Nτ are much higher in energy ($\Delta E \approx$ 250 kJ mol^{-1}), similar to isomers with two protons attached to Nπ (not shown).

Table 2 Relative energies (ΔE) and relative free energies ΔG (in kJ mol^{-1}) of the two most stable isomers of histamineH^+ (**A**, B) calculated at various levels of theory[a]

	ΔE		ΔG	
	A	**B**	**A**	**B**
B3LYP/cc-pVDZ	0.0	6.2	0.0	6.3
B3LYP/aug-cc-pVDZ	0.0	8.0	0.0	8.2
B3LYP/cc-pVTZ	0.0	9.1	0.0	9.2
B3LYP/aug-cc-pVTZ	0.0	9.2	0.0	9.4
B3LYP/cc-pVQZ	0.0	9.2	0.0	9.5
B3LYP/aug-cc-pVQZ	0.0	9.3	0.0	9.5
M06-2X/cc-pVDZ	0.0	3.6	0.0	3.7
M06-2X/aug-cc-pVDZ	0.0	5.5	0.0	5.6
M06-2X/cc-pVTZ	0.0	6.6	0.0	6.9
M06-2X/aug-cc-pVTZ	0.0	7.0	0.0	7.1
M06-2X/cc-pVQZ	0.0	7.4	0.0	7.7
M06-2X/aug-cc-pVQZ	0.0	7.5	0.0	7.7
MP2/cc-pVDZ	1.6	0.0	1.7	0.0
MP2/aug-cc-pVDZ	0.0	0.4	0.0	0.3
MP2/cc-pVTZ	0.0	1.0	0.0	0.9
MP2/aug-cc-pVTZ	0.0	1.0	0.0	0.9
MP2/cc-pVQZ	0.0	1.2	0.0	1.2
CCSD/cc-pVDZ	0.0	4.2	0.0	4.2
CCSD(T)/cc-pVDZ//CCSD/cc-pVDZ	0.0	0.3		
CBS-QB3	0.0	3.5	0.0	3.5

[a] Relative energies in this table include unscaled zero-point energy corrections.

Protonation at C atoms of the imidazole ring was not investigated, as previous MP2/6-311G(2df,2pd) calculations for imidazoleH^+ revealed that protonation at the basic N atom is favoured by around 150 kJ mol^{-1}.[84,85] Protonation at the aliphatic C atoms of the ethylamine side chain is expected to be even less favourable.[86] For completeness, we note that for all isomers depicted in Fig. 3 there are two symmetry-equivalent minima on the potential energy surface with the same energy obtained by reflection at the imidazole plane.[21] However, their interconversion involves relatively high barriers and the resulting tunnelling splittings are not resolved at the present spectral resolution. For example, in isomer **A** the two heavy atoms of the $–CH_2–NH_2$ unit in the side chain may either be above or below the aromatic plane. The barrier between these two equivalent minima amounts to 29.2 kJ mol^{-1} at the B3LYP/cc-pVDZ level. Thus, for all purposes of the present work, we can neglect the consequences of the existence of symmetry-equivalent enantiomers.

Interestingly, the energy difference between the two most stable isomers **A** and **B** is small and strongly depends on the theoretical level (Fig. 3, Table 2). Whereas the imidazolium ion **A** is calculated to be significantly more stable than the ammonium isomer **B** at the B3LYP/cc-pVDZ level (ΔE = 6.2 kJ mol^{-1}, ΔG = 6.3 kJ mol^{-1}), the reversed energetic order is predicted at the MP2/cc-pVDZ level, although with a much smaller energy gap (ΔE = 1.6 kJ mol^{-1}, ΔG = 1.7 kJ mol^{-1}). In an effort to address this important issue of the relative stability of these two isomers, their (free) energies are evaluated at a variety of theoretical levels and basis sets (Table 2). The differences between ΔE and ΔG are less than 0.3 kJ mol^{-1} at all theoretical levels considered, indicating that entropy effects are negligible for this problem. This result is expected because of the similar structures of both isomers. Density functional calculations using B3LYP and M06-2X show a

Table 3 Selected bond distances (in Å), bond and dihedral angles (in °), and relative energies and free energies at 298 K (in kJ mol^{-1}) of the two most stable isomers **A** and **B** of histamineH$^+$ and the transition state **TS** calculated at the B3LYP/cc-pVDZ and MP2/cc-pVDZ levels (Fig. 3 and Fig. S2 in ESI†)[a,b]

	A		**B**		**TS**	
	B3LYP	MP2	B3LYP	MP2	B3LYP	MP2
ϕ_1	−57.9	−59.4	−56.9	−59.4	−53.5	−55.9
ϕ_2	36.2	36.4	37.3	38.6	34.2	34.7
$R_{N\alpha\cdots H}$	1.790	1.742	1.106	1.092	1.271	1.342
$R_{N\pi\cdots H}$	1.059	1.065	1.587	1.614	1.309	1.238
$R_{N\tau\cdots H}$	1.016	1.019	1.015	1.018	1.015	1.018
$R_{N\pi\cdots N\alpha}$	2.659	2.626	2.586	2.592	2.491	2.485
θ	136.4	137.3	146.9	146.0	149.8	148.8
ΔE	0.0	1.6	6.2	0.0	10.4[c]	8.9[c]
ΔG	0.0	1.7	6.3	0.0		

[a] ϕ_1 = dihedral angle C5–C6–C7–Nα, ϕ_2 = dihedral angle Nπ–C5–C6–C7, θ = angle Nπ–H–Nα. [b] Corresponding data for the other isomers **C–J** are listed in Table S1 in ESI.† [c] Without zero-point energy corrections.

clear energetic preference for **A**, with energy gaps of ΔE = 9.3 and 7.5 kJ mol^{-1} using the aug-cc-pVQZ basis set, respectively. Interestingly, also the MP2 level preicts **A** to be more stable than **B** when using larger basis sets, although the energy gap is only of the order of 1 kJ mol^{-1} using the cc-pVQZ or aug-cc-pVTZ basis sets. Similarly, the CCSD(T)/cc-pVDZ//CCSD/cc-pVDZ level yields only a small energy preference for **A** (0.3 kJ mol^{-1}). In contrast, the popular CBS-QB3 level optimized for energy calculations arrives at a larger energy gap of ΔE = 3.5 kJ mol^{-1} in favour of **A**. In summary, all levels of theory considered in Table 2 predict **A** to be more stable than **B** when using sufficiently large basis sets, with energy differences ranging from 1 to 10 kJ mol^{-1}. Somewhat larger energy gaps are predicted at the density functional theory levels, whereas smaller gaps are obtained at correlated levels. Although high-level correlated calculations are required for establishing a more reliable energy difference between **A** and **B**, such calculations are not available in the literature, and beyond our computing resources and the scope of the present work.

As already noted, interconversion between **A** and **B** is achieved by simple proton transfer along the Nπ···H$^+$···Nα coordinate, which is accompanied by only modest structural rearrangements of the aromatic imidazole ring and the aliphatic side chain. Selected structural parameters for **A** and **B** and the transition state **TS** are listed in Table 3 and more details are given in Fig. S1 and S2 in ESI.† As can be seen, the main differences between both minima are related to the Nπ···H$^+$···Nα hydrogen bond. Calculations reveal that the barriers between both minima are of the order of 5–15 kJ mol^{-1} depending on the theoretical level and the direction of the proton shift. For example, the barriers are $V_{A\rightarrow B}$ = 10.4 and $V_{B\rightarrow A}$ = 4.6 kJ mol^{-1} at the B3LYP/cc-pVDZ level (see Fig. S3 in ESI† for a detailed potential energy surface scan). Single-point calculations using the larger aug-cc-pVDZ basis set yield slightly higher barriers of 13.9 and 10.0 kJ mol^{-1}, respectively. Similar values of 5.7 and 8.9 kJ mol^{-1} are obtained at the MP2/cc-pVDZ level, which again slightly increase to 10.0 and 11.2 kJ mol^{-1} using the larger aug-cc-pVDZ basis. Thus, although the barriers are modest, they are significant and large enough to support two separate minima in an asymmetric double-well potential. The strength of the H-bond in **A** can roughly be estimated as ~50 kJ mol^{-1} by the energy difference between the two isomers **D** and **A**. In a similar fashion, the stabilisation energy of the H-bond in **B** is estimated as ~70 kJ mol^{-1} by the energy difference between **F** and **B**. Indeed, the slightly stronger H-bond in **B** is consistent with a shorter NH$^+$···N bond distance as compared to **A** (1.59 *vs.* 1.79 Å). The Nπ···Nα distances in **A** and **B** are relatively large (2.66 and 2.59 Å) and the H-bonds are deviating significantly from linearity (θ = 136° and 147°). As expected, the Nπ···Nα distance is shortest at **TS** (2.49 Å), and the Nπ···H$^+$···Nα hydrogen bridge is slightly asymmetric, with the Nα–H bond being slightly shorter than the Nπ–H bond at the B3LYP level (1.27 *vs.* 1.31 Å) and the reversed situation at the MP2 level (1.34 *vs.* 1.24 Å). All these observations are consistent with the moderate ionic H-bond strengths in both isomers and in line with the clear formation of a double-well potential separating the two minima **A** and **B** by an appreciable barrier. For comparison, although the more strongly bound protonated ammonia dimer, $N_2H_7^+$, features a much stronger linear N–H$^+$···N hydrogen bond with D_0 ≈ 110 kJ mol^{-1}, the potential still features a symmetric double minimum potential with a barrier of 4 kJ mol^{-1}.[87]

The NBO population analysis for the isomers **A** and **B** of histamineH$^+$ is detailed in Fig. S4 in ESI.† In isomer **A**, most of the additional positive charge is distributed over the imidazole ring system (+0.84 e), and only little charge is located on the ethylamine side chain (+0.16 e), consistent with the view of an imidazolium ion. The situation is reversed in **B**, with most of the excess charge located on the protonated ethylamine side chain (+0.88 e) and little charge on the heterocyclic ring (+0.12 e), consistent with the notion of an ammonium ion. In both isomers, the proton in the Nπ···H$^+$···Nα hydrogen bond carries high positive partial charge (~0.5 e). In **TS**, the excess proton also carries +0.49 e and the rest of the positive charge is nearly equally distributed between the imidazole (+0.21 e) and ethylamine chain (+0.31 e), as expected for an intermediate between an imidazolium and an ammonium ion.

In the next step, we compare in Fig. 5 the measured IRMPD spectrum of histamineH$^+$ to linear IR absorption spectra calculated for the low-energy isomers **A–F** shown in Fig. 3. IR spectra of the less stable isomers with ΔE > 100 kJ mol^{-1} are reproduced in Fig. S5 of ESI.† For this purpose, we employ spectra derived at the B3LYP level, because this theoretical approach has shown to provide reliable IR spectra of protonated aromatic molecules and their complexes,[68–70,74] including the related protonated neurotransmitter molecules serotoninH$^+$ and dopamineH$^+$.[12,13] In contrast, MP2 calculations often fail to properly reproduce IR spectra of (protonated) aromatic molecules.[68,70,88]

Inspection of Fig. 5 immediately reveals satisfactory correspondence between the measured IRMPD spectrum of histamineH$^+$ and the spectrum calculated for the most stable isomer **A**, with respect to both peak positions and relative intensities. At this stage, one has to bear in mind that the

multiple photonic nature of the IRMPD process may cause minor but noticeable deviations from a linear IR absorption spectrum, such as modest red shifts of 10–30 cm^{-1} and slight modifications of relative IR intensities of close-lying vibrational resonances.[36,82] Both effects are visible here and discussed in more detail below. Clearly, the agreement between the IRMPD spectrum and the IR spectrum calculated for **B** is much worse as compared to **A**. For example, the very intense NH bend vibration (β_{NH}) of the ammonium group predicted at 1480 cm^{-1} is not visible in the measured spectrum, suggesting at most only minor population of **B** in the sampled histamineH^+ ion cloud. Actually, anharmonic calculations discussed below predict the intense β_{NH} transition to occur near 1400 cm^{-1}, again in a spectral range where only little intensity is detected in the experimental spectrum. Further features of the IRMPD spectrum, which are not reproduced by the calculated spectrum of **B**, include the intense G/H doublet and the high intensity of bands B and O. In addition, the spectrum of **B** predicts an intense band near 1250 cm^{-1}, which is completely absent in the measured spectrum. All these observations suggest that **B** does not provide major contributions to the experimental IRMPD spectrum. The same conclusion holds also for the higher lying isomers **C–J** (Fig. 5 and Fig. S5 in ESI†). As an example, the spectra of **C–J** all lack the intense G/H doublet detected in the IRMPD spectrum.

In addition to spectroscopic arguments, thermodynamic considerations support the assignment of the spectrum mainly to isomer **A**. Assuming thermodynamic equilibrium, a temperature of 300 K, and a free energy difference of 5 kJ mol^{-1} between **A** and **B**, the Boltzmann population of **B** is expected to be of the order of only 10%. As the ESI process is quite energetic and the barriers for interconversion between **A** and **B** are quite low, the assumption of thermodynamic rather than kinetic control seems to be a realistic hypothesis for estimating the formation ratio of the two histamineH^+ isomers in the ESI source connected to the hexapole trap used for ion accumulation and thermalization. The spectra in Fig. 5 suggest that the contribution of **B** to the IRMPD spectrum is well below 30%. This translates in a minimum energy gap of $\Delta G = 2.5$ kJ mol^{-1} between **A** and **B**.

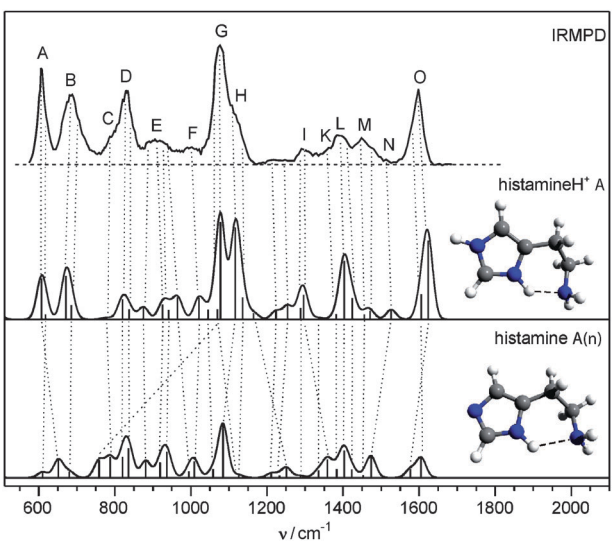

Fig. 6 Comparison of the IRMPD spectrum of histamineH^+ with the linear IR absorption spectra of the most stable isomers of histamineH^+ (**A**) and neutral histamine (**A(n)**) calculated at the B3LYP/cc-pVDZ level (Table 1).

On the basis of thermodynamic and spectroscopic considerations, isomer **A** is clearly identified as the major carrier of the measured IRMPD spectrum. Hence, the vibrational assignment of the observed transitions in Table 1 is to normal modes of **A**. This table compares the peak positions of the IRMPD spectrum of histamineH^+ with the vibrational frequencies and IR intensities calculated for isomer **A** of histamineH^+ and isomer **A(n)** of neutral histamine in the considered 600–1650 cm^{-1} frequency range. The corresponding IR spectra are directly compared in Fig. 6. Several bands in the IRMPD spectrum of histamineH^+ correspond mainly to single, relatively intense transitions calculated for isomer **A** (*e.g.*, bands A, B, G, H, L, and O), whereas other bands are due to more than one significant vibrational mode. The maximum deviation of the positions of the experimental band maxima from the frequencies calculated for **A** is 25 cm^{-1}, with an average deviation of less than 16 cm^{-1}. This result confirms the vibrational and isomer assignments given in Table 1. In addition, all modes with calculated oscillator strengths larger than ~10–15 km mol^{-1} are visible in the experimental spectrum. This threshold intensity is typical for IRMPD detection of molecular ions of this size.[70]

Band A at 607 cm^{-1} in the IRMPD spectrum is assigned to an out-of-plane ring deformation mode of imidazole, corresponding to ν_{19}(Im). Band B at 685 cm^{-1} is attributed to the out-of-plane NH bend (γ_{NH}) at Nτ, a mode which is absent for neutral **A(n)**. Transition D at 830 cm^{-1} arises from an out-of-plane CH bend (γ_{CH}) of the imidazole ring, ν_{16}(Im). The weak bands E and F at 909 and 997 cm^{-1} are mainly assigned to the imidazole ring stretching modes ν_{15}(Im) and ν_{14}(Im), respectively. The intense band G at 1075 cm^{-1} is attributed to the out-of-plane NH bend (γ_{NH}) at Nπ, *i.e.* a proton motion perpendicular to the Nπ–$H^+\cdots$Nα hydrogen bond. Since the H-bond is much stronger in the protonated species, this mode experiences a large blueshift compared to neutral **A(n)** from 758 to 1078 cm^{-1}. Also the IR intensity is substantially enhanced from 21 to 117 km mol^{-1} in the ionic species. The shoulder H at 1107 cm^{-1} arises from the in-plane NH bend (β_{NH}) of the proton at Nπ, corresponding to ν_{12}(Im). Interestingly, the blueshift of this mode upon protonation from 1084 to 1117 cm^{-1} is much smaller than for γ_{NH}. The weak transition I at 1293 cm^{-1} is assigned to a highly-coupled mode, delocalized over imidazole and the alkylamine side chain (Table 1). Band L at 1389 cm^{-1} is mainly due to ν_7(Im). Band M at 1453 cm^{-1} is dominated by the in-plane NH bend (β_{NH}) at Nτ, a mode which is again absent in neutral **A(n)**. Finally, the main intensity of band O at 1598 cm^{-1} arises from the ν_5(Im) ring mode, with a smaller contribution in the red wing coming from the NH_2 scissoring mode of the terminal amino group.

In general, there is satisfactory agreement between the measured IRMPD spectrum and the linear absorption spectrum calculated for **A**. There are, however, several notable discrepancies, most of which can be attributed to the multiple photonic nature of the IRMPD process. First, although the

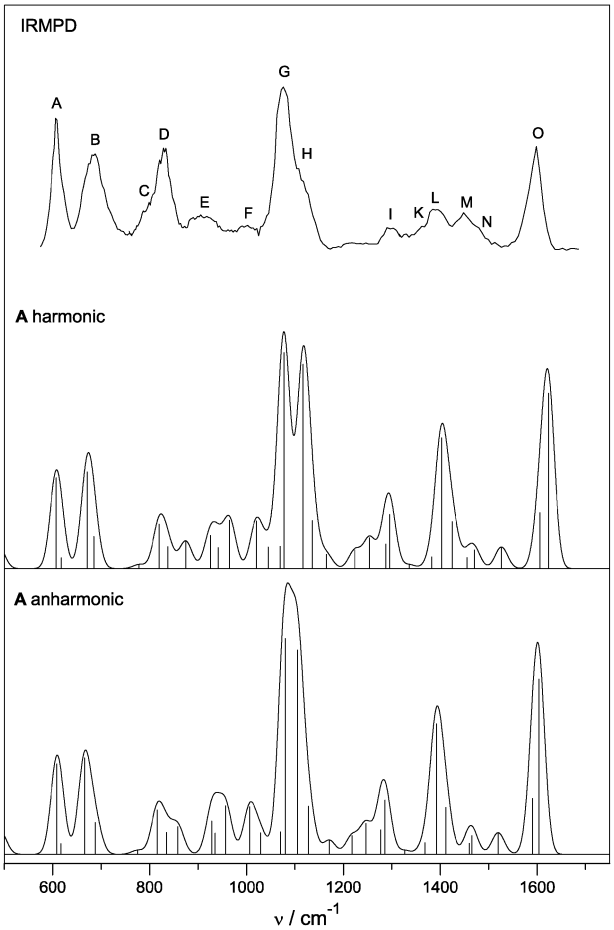

Fig. 7 Comparison of the IRMPD spectrum of histamineH^+ with IR spectra of isomer **A** using the harmonic (scaling factor 0.98) and anharmonic approximation.

IRMPD technique reflects mainly the absorption of the first photon and thus justifies in zero-order direct comparison with a linear absorption spectrum, a certain threshold intensity I_{th} of the vibrational transition is required to allow for its detection. In the present case, I_{th} lies near 10–15 km mol^{-1}. A second effect of the IRMPD process on the IR spectrum of a molecule are redshifts of the transitions due to anharmonic vibrational couplings. Depending on the vibrational mode of the molecular ion, this redshift typically varies between 10 and 30 cm^{-1} in the fingerprint range. It can often be absorbed in the scaling factor, which is then slightly lower than that obtained when considering a linear IR spectrum. Nonetheless, for heavily affected modes this redshift may not fully be compensated for by the scaling factor, as is seen here for the intense ν_5(Im) mode (band O), which appears in the IRMPD spectrum 25 cm^{-1} lower than the value predicted after scaling. A further side effect of anharmonic coupling is that IRMPD intensities for two close-lying transitions are modified such that the lower-frequency mode gains intensity. One such example in the IRMPD spectrum of histamineH^+ is the doublet G/H.

Several vibrational modes related to the intramolecular N$\pi\cdots H^+\cdots$Nα H-bond in the isomers **A** and **B** exhibit rather large anharmonicity, which is not adequately compensated for by using a scaling factor applied to harmonic frequencies. In an effort to estimate the effects of anharmonicity on the IR spectra in a more sophisticated fashion, anharmonic frequencies are determined at the B3LYP/cc-pVDZ level using the procedure implemented in GAUSSIAN09. The resulting anharmonic spectra are compared in Fig. S6 in ESI† directly to those obtained by harmonic calculations treated with a scaling factor. For isomer **A**, both IR spectra are very similar in the considered fingerprint range (500–2000 cm^{-1}), indicating that the application of a scaling factor to harmonic spectra provides a reliable description of the IR spectrum of **A** in this spectral range. In fact, the agreement of the IRMPD spectrum with the calculated anharmonic spectrum appears to be better than with the scaled harmonic spectrum (Fig. 7), in particular concerning the position of band O and the splitting between bands G and H. As expected, the Nπ–H proton donor stretch mode (σ_{NH}) is the vibration with the largest frequency shift upon taking anharmonicity into account, leading to a reduction from 2860 to 2376 cm^{-1} (Fig. S6 in ESI†). The latter value is still outside the scanned range and does not affect the comparison of the spectra in Fig. 5 and 7. In contrast, the spectrum of isomer **B** is significantly modified in the 500–2000 cm^{-1} range when anharmonicity is included (Fig. S6 in ESI†). First, the Nα–H proton donor stretch mode (σ_{NH}) is redshifted from 2260 to 1317 cm^{-1} and dominates the calculated spectrum of **B** in the range considered for the IRMPD spectrum. Second, the frequency of the Nα–H in-plane bend (β_{NH}) is also reduced from 1476 to 1403 cm^{-1}. These modifications to the simulated IR spectrum of **B** predict two very intense transitions near 1300 and 1400 cm^{-1}, in large disagreement with the experimental IRMPD spectrum. This result may be taken as further evidence that isomer **B** does not significantly contribute to the IRMPD spectrum.

In an effort to estimate the effects of the possibly large amplitude motion of the proton in the N$\pi\cdots H^+\cdots$Nα bridge, the IR spectra of **A**, **B**, and **TS** are compared in Fig. S7 in ESI.† This comparison suggests that the excess proton is indeed largely localized on the imidazole moiety. Although the spectra of **A** and **TS** are quite similar in most parts of the spectral range considered, the spectrum of **A** reproduces the G/H double peak, whereas the spectrum of **TS** does not.

At this stage, it is interesting to realize that the ESI-generated histamineH^+ isomer identified by IRMPD in the gas phase (**A**) is different from those found in solution, which are *gauche* and *trans* isomers of Nα-protonated Nτ and Nπ tautomers.[5,9,17,18] As already mentioned, the stabilization induced by solvation of the ammonium group in aqueous solution overrides the effects of intramolecular H-bonding to the imidazolium ion. This observation implies that during the ESI process, the proton is transferred from Nα to Nπ. As this simple proton transfer occurs *via* a low barrier along the N$\pi\cdots H^+\cdots$Nα coordinate and involves only little structural rearrangements of the imidazole ring and the aliphatic side chain, it may readily occur during the ESI process.

In line with low-energy collision-induced dissociation (CID) experiments,[89] the only significant fragment observed upon IRMPD of histamineH^+ (m/z = 112) corresponds to elimination of NH_3, leading to a fragment ion with m/z = 95. Since both dissociation processes, CID and IRMPD, occur on the

Table 4 Selected bond lengths (Å) and angles (°) of the **A(n)** and **A** isomers of neutral and protonated histamine (Fig. 6) evaluated at the B3LYP/cc-pVDZ level[a]

Bond	Histamine **A(n)**	HistamineH$^+$ **A**	Δ^b	Angle	Histamine **A(n)**	HistamineH$^+$ **A**	Δ^b
Nπ–C2	1.365	1.331	−0.034	Nπ–C2–Nτ	111.9	107.3	−4.6
C2–Nτ	1.320	1.341	0.021	C2–Nτ–C4	104.9	109.8	4.9
Nτ–C4	1.379	1.385	0.006	Nτ–C4–C5	111.0	106.5	−4.5
C4–C5	1.381	1.373	−0.008	C4–C5–Nπ	104.6	106.2	1.6
C5–Nπ	1.381	1.386	0.005	C5–Nπ–C2	107.5	110.2	2.7
C5–C6	1.500	1.501	0.001	Nπ–C5–C6–C7	42.5	36.2	−6.3
C6–C7	1.537	1.541	0.004	C5–C6–C7–Nα	−64.2	−57.9	6.3
C7–Nα	1.477	1.484	0.007				
Nα–H	2.140	1.790	−0.350				
Nπ–H	1.020	1.059	0.039				
Nτ–H		1.016					

[a] Further values are provided in Fig. S10 in ESI.† [b] Δ denotes the structural change upon protonation, **A–A(n)**.

ground electronic state, NH_3 loss appears to be the lowest-energy fragment channel. In an effort to identify plausible structures of the m/z = 95 fragment, several possible isomers are calculated at the B3LYP/cc-pVDZ level. The six considered structures denoted **FN_95** with N = I–VI are shown in Fig. S8 in ESI†, along with their relative energies and dissociation energies for NH_3 loss. The three lowest-energy structures considered **FI_95–FIII_95** are methylated protonated 1,3-diazine ions, which are very similar in structure, energy, and binding energy. However, their formation probably involves high activation barriers, because NH_3 loss is followed by an expansion of the five-membered imidazole ring to a six-membered diazine ring. Thus, the most likely structure of the m/z = 95 fragment is believed to be **FIV_95**, which is 75 kJ mol^{-1} higher in energy than **FI_95** but can readily be generated by a simple H-shift after NH_3 elimination. At the present stage, it is however difficult to safely identify the actual structure of the fragment ion observed in the IRMPD experiment. Further mass spectrometric and spectroscopic experiments[90] for the m/z = 95 ion to confirm its structure are beyond the scope of the present work.

3.2 Effects of protonation

To evaluate the effects of protonation, we compare the properties of the most stable isomer of histamineH$^+$ (**A**) with those of the most stable structure **A(n)** of neutral histamine identified by microwave spectroscopy,[26,27] and the current quantum chemical calculations (Fig. S9 in ESI†). In this comparison, **A** is generated from **A(n)** by adding a proton to Nτ of the imidazole ring (Fig. 6). Both structures are significantly stabilized by intramolecular Nπ–H$^{(+)}\cdots$Nα hydrogen bonds, although the strength of the ionic H-bond is roughly five times stronger (~70 kJ mol^{-1}) than in the neutral species (~10–20 kJ mol^{-1}, Fig. S9 in ESI†).[27] The energy difference between **A** and **A(n)** corresponds to the proton affinity of histamine and amounts to 1005.4 (1007.0) kJ mol^{-1} at the B3LYP(MP2)/cc-pVDZ levels. These values compare favourably with the tabulated experimental value of 999.8 kJ mol^{-1},[29,91] although the latter value is not isomer specific.

Selected structural parameters of **A** and **A(n)** are compared in Table 4 and Fig. S10 in ESI.† The rotational constants calculated for **A(n)** (A_e = 4934 MHz, B_e = 1395 MHz, C_e = 1138 MHz) agree well with those measured for the most stable species by microwave spectroscopy (A_0 = 4952 MHz, B_e = 1392 MHz, C_e = 1141 MHz),[26] confirming that the B3LYP/cc-pVDZ reliably describes its structure. Fig. S11 in ESI† provides details of the NBO charge distribution in **A** and **A(n)**. As expected, in neutral **A(n)** both the imidazole ring and the side chain are essentially neutral. As already mentioned, addition of the proton to Nτ implies that the imidazole ring in **A** carries nearly all positive charge (+0.84 e), with an increase of 0.05 e of the positive partial charge on the proton in the intramolecular Nπ–H$^{(+)}\cdots$Nα H-bond. This drastic change in the charge distribution is responsible for the substantial increase in the strength of the H-bond upon protonation. The ionic H-bond is much shorter than the neutral one (1.79 *vs.* 2.14 Å) and more linear (θ = 136 *vs.* 126°). As a consequence of the stronger H-bond in **A**, the Nπ–H proton donor bond is elongated in **A** by 0.04 Å. Of course, protonation of the imidazole ring also affects its geometry, and the main bond length changes include a contraction of the Nπ–C2 bond (0.034 Å) and an elongation of the neighbouring C2–Nτ bond (0.021 Å). All other bond length changes are less than 0.01 Å, and particularly the geometry changes of the ethylamine side chain are modest.

The structural changes upon protonation directly translate into differences in the vibrational spectra of **A** and **A(n)**. As no experimental IR spectrum is available for free histamine, comparison can only be performed between the calculated spectra (Fig. 6, Table 1). The major differences are briefly discussed. The excess proton attached to Nτ gives rise to two additional fundamentals in the fingerprint range, namely the out-of-plane and in-plane NH bends at γ_{NH} = 671 and β_{NH} = 1471 cm^{-1}. The γ_{NH} mode is experimentally observed as an intense isolated transition at 685 cm^{-1} (band B), whereas β_{NH} is weakly seen at 1453 cm^{-1} (band M). The in-plane CC stretch mode ν_5(Im) increases in frequency by 46 cm^{-1} from 1577 to 1623 cm^{-1}, due to the protonation-induced contraction of the C4C5 bond, and is detected as intense band O at 1598 cm^{-1}. Similarly, the ν_6(Im) frequency increases by 53 cm^{-1} from 1474 to 1527 cm^{-1} (band N at 1515 cm^{-1}) because of the substantial contraction of the C2–Nπ bond upon protonation. As a consequence of the drastic increase in the intramolecular H-bond strength, the frequencies of the in-plane and out-of-plane NH bends (β_{NH} and γ_{NH}) of the Nπ–H$^+\cdots$Nα proton bridge shift significantly to higher frequency and appear with enhanced IR intensity. The effect is much larger for γ_{NH}

(758 → 1078 cm^{-1}), which is observed as intense band G at 1075 cm^{-1}. The blueshift for the β_{NH} transition is less pronounced (1084 → 1117 cm^{-1}), and the band is observed at 1107 cm^{-1} (band H). The fact that the experimental IRMPD spectrum reproduces these β/γ_{NH} frequencies to within 10 cm^{-1} provides evidence that the B3LYP/cc-pVDZ level describes the intramolecular Nπ–H^+···Nα H-bond to satisfactory accuracy. Further noticeable redshifts upon protonation include $\Delta\nu_{19}$(Im) = −45 cm^{-1} for the out-of-plane ring deformation (652 → 607 cm^{-1}) experimentally observed at 607 cm^{-1} (band A), and a highly coupled mode giving rise to band I at 1293 cm^{-1} (1359 → 1296 cm^{-1}, $\Delta\nu$ = −63 cm^{-1}). Comparison of the spectrum calculated for **A(n)** with that taken from the NIST data base[86] is provided in Fig. S12 in ESI.† The NIST spectrum is a solid-state spectrum taken in mineral oil mull and partly contaminated by oil resonances. In any case, it looks different in appearance from that predicted for **A(n)** consistent with the hypothesis that gas and condensed phase structures are different for histamine(H^+).

4. Concluding remarks

The IRMPD spectrum of isolated histamineH^+ recorded in the fingerprint range, in combination with quantum chemical calculations, provides the first experimental information about the tautomeric and conformational structure of this fundamental protonated neurotransmitter molecule in the gas phase. The experimental spectrum is consistent with isomer **A** being by far the dominant carrier. This imidazolium-type isomer is calculated to be the most stable isomer of histamineH^+. Protonation occurs at the basic N atom of the imidazole ring, and the resulting imidazolium ion is substantially stabilized by an intramolecular Nπ–H^+···Nα hydrogen bond (~50 kJ mol^{-1}) to the lone pair of the terminal amino group of the aliphatic ethylamine side chain in *gauche* conformation. Significantly, the structure found in the gas phase is different from those identified in the liquid and crystalline phases, which all are protonated at the amino group leading to ammonium isomers in *gauche* and/or *trans* conformation. This difference emphasizes the important effects of solvation and counter ions on the structure of histamineH^+. The lowest-energy ammonium isomer of isolated histamineH^+ (isomer **B**) can be derived from **A** by simple proton transfer along the Nπ–H^+···Nα proton bridge involving barriers of 5–15 kJ mol^{-1}. Although the energy difference between **A** and **B** is calculated to be small (1–10 kJ mol^{-1} depending on the level of theory), the experimental IRMPD spectrum does not show any conclusive evidence for the presence of isomer **B**, suggesting only minor population in the sampled ion cloud. Clearly, higher-level calculations and multidimensional anharmonic calculations are required to reliably determine the free energy profile of this interesting proton-transfer double-well potential connecting **A** and **B** with high accuracy. The established structural transition from an imidazolium to an ammonium ion upon aqueous solvation makes histamineH^+ an ideal target for spectroscopic characterization of microhydrated histamineH^+ clusters, histamineH^+–$(H_2O)_n$, in order to follow the proton transfer upon hydration in a stepwise fashion by systematically increasing *n*. Similarly, the small barriers for proton transfer and the large effects of anharmonicity make isolated and microhydrated histamineH^+ an attractive model system for molecular dynamic simulations to evaluate the effects of temperature, anharmonicity, and (micro-)solvation on structure, energy, and the appearance of the IR spectrum.[92] Finally, spectroscopic studies of histamineH^+–$(H_2O)_n$ and their deuterated species in the NH and OH stretch range[85,93] will provide further insight into the structure and energetics of the intra- and intermolecular H-bonds in these biophysically interesting species. Comparison between histamineH^+ and histamine reveals the effects of protonation on the structure, energy, intramolecular hydrogen bonding, and IR spectrum. Unfortunately, IR spectra of neutral histamine are lacking so far though recent progress toward IR spectroscopy of non-volatile neutral neurotransmitters in molecular beams will change this situation in the near future.[94,95] In general, the results for histamineH^+ are similar to conclusions for the related histidineH^+ molecule reached from mass spectrometry and quantum chemistry,[96] although (IR) spectra of the protonated amino acid analogue in the gas phase have not been reported yet.

Acknowledgements

This work was supported by Technische Universität Berlin, Deutsche Forschungsgemeinschaft (DO 729/3), and the European Community (FP7/2007-2013, grant 226716). We gratefully acknowledge the excellent assistance by the FELIX staff (B. Redlich *et al.*).

References

1 M. A. Medina, J. L. Urdiales, C. Rodriguez-Caso, F. J. Ramirez and F. Sanchez-Jimenez, *Crit. Rev. Biochem. Mol. Biol.*, 2003, **38**, 23–59.
2 J. C. Schwartz, H. Pollard and T. T. Quach, *J. Neurochem.*, 1980, **35**, 26–33.
3 L. Stryer, *Biochemistry*, Freeman, New York, 1996.
4 O. B. Reite, *Physiol. Rev.*, 1972, **52**, 778–819.
5 C. R. Ganellin, E. S. Pepper, G. N. J. Port and W. G. Richards, *J. Med. Chem.*, 1973, **16**, 610–616.
6 C. R. Ganellin, G. N. J. Port and W. G. Richards, *J. Med. Chem.*, 1973, **16**, 616–620.
7 C. R. Ganellin, *J. Med. Chem.*, 1973, **16**, 620–623.
8 C. R. Ganellin, *J. Pharm. Pharmacol.*, 1973, **25**, 787–792.
9 T. B. Paiva, M. Tominaga and A. C. M. Paiva, *J. Med. Chem.*, 1970, **13**, 689–692.
10 D. A. Dougherty, *Science*, 1996, **271**, 163–168.
11 T. D. Vaden, T. de Boer, J. P. Simons and L. C. Snoek, *Phys. Chem. Chem. Phys.*, 2008, **10**, 1443–1447.
12 A. Lagutschenkov, J. Langer, G. Berden, J. Oomens and O. Dopfer, *Phys. Chem. Chem. Phys.*, 2011, **13**, 2815–2823.
13 A. Lagutschenkov, J. Langer, G. Berden, J. Oomens and O. Dopfer, *J. Phys. Chem. A*, 2010, **114**, 13268–13276.
14 K. Prout, S. R. Critchle and C. R. Ganellin, *Acta Crystallogr., Sect. B: Struct. Sci.*, 1974, **30**, 2884–2886.
15 J. A. Collado and F. J. Ramirez, *J. Raman Spectrosc.*, 1999, **30**, 391–397.
16 J. J. Bonnet and J. A. Ibers, *J. Am. Chem. Soc.*, 1973, **95**, 4829–4833.
17 A. F. Casy, R. R. Ison and N. S. Ham, *J. Chem. Soc. D*, 1970, 1343–1344.
18 J. A. Collado, I. Tunon, E. Silla and F. J. Ramirez, *J. Phys. Chem. A*, 2000, **104**, 2120–2131.
19 R. E. Wasylishen and G. Tomlinson, *Can. J. Biochem.*, 1977, **55**, 579–582.
20 F. J. Ramirez, I. Tunon, J. A. Collado and E. Silla, *J. Am. Chem. Soc.*, 2003, **125**, 2328–2340.
21 P. I. Nagy, G. J. Durant, W. P. Hoss and D. A. Smith, *J. Am. Chem. Soc.*, 1994, **116**, 4898–4909.

22 P. I. Nagy, G. J. Durant, W. P. Hoss and D. A. Smith, *J. Am. Chem. Soc.*, 1994, **116**, 7957.
23 G. Karpinska, J. C. Dobrowolski and A. P. Mazurek, *THEOCHEM*, 1996, **369**, 137–144.
24 Y. G. Smeyers, F. J. Romero-Sanchez and A. Hernandez-Laguna, *THEOCHEM*, 1985, **24**, 431–442.
25 W. G. Richards, J. Wallis and C. R. Ganellin, *Eur. J. Med. Chem.*, 1979, **14**, 9–12.
26 B. Vogelsanger, P. D. Godfrey and R. D. Brown, *J. Am. Chem. Soc.*, 1991, **113**, 7864–7869.
27 P. D. Godfrey and R. D. Brown, *J. Am. Chem. Soc.*, 1998, **120**, 10724–10732.
28 A. Hernandez-Laguna, J. L. M. Abboud, R. Notario, H. Homan and Y. G. Smeyers, *J. Am. Chem. Soc.*, 1993, **115**, 1450–1454.
29 M. Decouzon, J. F. Gal, P. C. Maria and E. D. Raczynska, *Rapid Commun. Mass Spectrom.*, 1993, **7**, 599–602.
30 A. Hernandez-Laguna, Z. Cruz-Rodriguez, Y. G. Smeyers, G. A. Arteca, J. L. M. Abboudd and O. Tapia, *THEOCHEM*, 1995, **335**, 77–87.
31 A. Hernandez-Laguna, Z. Cruz-Rodriguez and R. Notario, *J. Mol. Struct.*, 1998, **433**, 247–262.
32 E. D. Raczynska, M. Darowska, M. K. Cyranski, M. Makowski, T. Rudka, J. F. Gal and P. C. Maria, *J. Phys. Org. Chem.*, 2003, **16**, 783–796.
33 E. D. Raczynska, M. Darowska, T. Rudka and M. Makowski, *J. Phys. Org. Chem.*, 2001, **14**, 770–777.
34 J. V. Correa, B. Herrera and A. Toro-Labbe, *J. Mol. Struct.*, 2007, **817**, 111–118.
35 O. Dopfer, *J. Phys. Org. Chem.*, 2006, **19**, 540–551.
36 J. Oomens, B. G. Sartakov, G. Meijer and G. Von Helden, *Int. J. Mass Spectrom.*, 2006, **254**, 1–19.
37 E. J. Bieske and O. Dopfer, *Chem. Rev.*, 2000, **100**, 3963–3998.
38 O. Dopfer, *Int. Rev. Phys. Chem.*, 2003, **22**, 437.
39 O. Dopfer, *Z. Phys. Chem.*, 2005, **219**, 125.
40 N. Solca and O. Dopfer, *Chem. Phys. Lett.*, 2001, **342**, 191–199.
41 N. Solca and O. Dopfer, *J. Chem. Phys.*, 2004, **120**, 10470–10482.
42 N. Solca and O. Dopfer, *J. Am. Chem. Soc.*, 2004, **126**, 1716–1725.
43 N. Solca and O. Dopfer, *Angew. Chem., Int. Ed.*, 2002, **41**, 3628–3631.
44 N. Solca and O. Dopfer, *Chem.–Eur. J.*, 2003, **9**, 3154–3163.
45 G. E. Douberly, A. M. Ricks, P. V. R. Schleyer and M. A. Duncan, *J. Phys. Chem. A*, 2008, **112**, 4869–4874.
46 A. M. Ricks, G. E. Douberly and M. A. Duncan, *Astrophys. J.*, 2009, **702**, 301–306.
47 F. Pasker, N. Solcà and O. Dopfer, *J. Phys. Chem. A*, 2006, **110**, 12793–12804.
48 N. Solca and O. Dopfer, *ChemPhysChem*, 2005, **6**, 434–436.
49 H. S. Andrei, N. Solca and O. Dopfer, *ChemPhysChem*, 2006, **7**, 107–110.
50 N. Solcà and O. Dopfer, *Angew. Chem., Int. Ed.*, 2003, **42**, 1537.
51 N. Solca and O. Dopfer, *J. Am. Chem. Soc.*, 2003, **125**, 1421–1430.
52 S. Chakraborty, A. Patzer and O. Dopfer, *J. Chem. Phys.*, 2010, **133**, 044307.
53 N. Solca and O. Dopfer, *J. Chem. Phys.*, 2004, **121**, 769–772.
54 N. A. Macleod and J. P. Simons, *Phys. Chem. Chem. Phys.*, 2004, **6**, 2821–2826.
55 N. A. Macleod and J. P. Simons, *Mol. Phys.*, 2006, **104**, 3317–3328.
56 T. D. Vaden, T. de Boer, N. A. MacLeod, E. M. Marzluff, J. P. Simons and L. C. Snoek, *Phys. Chem. Chem. Phys.*, 2007, **9**, 2549–2555.
57 W. Jones, P. Boissel, B. Chiavarino, M. E. Crestoni, S. Fornarini, J. Lemaire and P. Maitre, *Angew. Chem., Int. Ed.*, 2003, **42**, 2057.
58 J. Oomens, G. von Helden and G. Meijer, *J. Phys. Chem. A*, 2004, **108**, 8273.
59 O. Dopfer, J. Lemaire, P. Maitre, M. E. Crestoni and S. Fornarini, *Int. J. Mass Spectrom.*, 2006, **249–250**, 149–154.
60 U. J. Lorenz, J. Lemaire, P. Maitre, M. E. Crestoni, S. Fomarini and O. Dopfer, *Int. J. Mass Spectrom.*, 2007, **267**, 43–53.
61 U. J. Lorenz, N. Solca, J. Lemaire, P. Maitre and O. Dopfer, *Angew. Chem., Int. Ed.*, 2007, **46**, 6714–6716.
62 B. Chiavarino, M. E. Crestoni, S. Fornarini, O. Dopfer, J. Lemaire and P. Maitre, *J. Phys. Chem. A*, 2006, **110**, 9352.
63 O. Dopfer, N. Solcà, J. Lemaire, P. Maitre, M. E. Crestoni and S. Fornarini, *J. Phys. Chem. A*, 2005, **109**, 7881.
64 N. C. Polfer and J. Oomens, *Mass Spectrom. Rev.*, 2009, **28**, 468–494.
65 J. R. Eyler, *Mass Spectrom. Rev.*, 2009, **28**, 448–467.
66 M. Seydou, G. Gregoire, J. Liquier, J. Lemaire, J. P. Schermann and C. Desfrancois, *J. Am. Chem. Soc.*, 2008, **130**, 4187–4195.
67 T. D. Fridgen, *Mass Spectrom. Rev.*, 2009, **28**, 586–607.
68 D. W. Zhao, J. Langer, J. Oomens and O. Dopfer, *J. Chem. Phys.*, 2009, **131**, 184307.
69 H. Knorke, J. Langer, J. Oomens and O. Dopfer, *Astrophys. J. Lett.*, 2009, **706**, L66–L70.
70 A. Lagutschenkov and O. Dopfer, *J. Mol. Spectrosc.*, 2011, DOI: 10.1016/j.jms.2011.1003.1024, in press.
71 H. A. Galue, O. Pirali and J. Oomens, *Astron. Astrophys.*, 2010, **517**, 11.
72 J. M. Bakker, T. Besson, J. Lemaire, D. Scuderi and P. Maitre, *J. Phys. Chem. A*, 2007, **111**, 13415–13424.
73 L. MacAleese and P. Maitre, *Mass Spectrom. Rev.*, 2007, **26**, 583–605.
74 S. Chakraborty and O. Dopfer, *ChemPhysChem*, 2011, **12**, 1999–2008.
75 A. Lagutschenkov, A. Springer, U. J. Lorenz, P. Maitre and O. Dopfer, *J. Phys. Chem. A*, 2010, **114**, 2073–2079.
76 A. Lagutschenkov, R. K. Sinha, P. Maitre and O. Dopfer, *J. Phys. Chem. A*, 2010, **114**, 11053–11059.
77 T. R. Rizzo, J. A. Stearns and O. V. Boyarkin, *Int. Rev. Phys. Chem.*, 2009, **28**, 481–515.
78 N. S. Nagornova, T. R. Rizzo and O. V. Boyarkin, *J. Am. Chem. Soc.*, 2010, **132**, 4040.
79 J. A. Stearns, S. Mercier, C. Seaiby, M. Guidi, O. V. Boyarkin and T. R. Rizzo, *J. Am. Chem. Soc.*, 2007, **129**, 11814–11820.
80 D. Oepts, A. F. G. Van der Meer and P. W. Van Amersfoort, *Infrared Phys. Technol.*, 1995, **36**, 297–308.
81 J. J. Valle, J. R. Eyler, J. Oomens, D. T. Moore, A. F. G. van der Meer, G. von Helden, G. Meijer, C. L. Hendrickson, A. G. Marshall and G. T. Blakney, *Rev. Sci. Instrum.*, 2005, **76**, 7.
82 J. Oomens, A. Tielens, B. G. Sartakov, G. von Helden and G. Meijer, *Astrophys. J.*, 2003, **591**, 968–985.
83 M. J. T. Frisch, G. W. Trucks, H. B. Schlegel, G. E. Scuseria, M. A. Robb, J. R. Cheeseman, G. Scalmani, V. Barone, B. Mennucci, G. A. Petersson, H. Nakatsuji, M. Caricato, X. Li, H. P. Hratchian, A. F. Izmaylov, J. Bloino, G. Zheng, J. L. Sonnenberg, M. Hada, M. Ehara, K. Toyota, R. Fukuda, J. Hasegawa, M. Ishida, T. Nakajima, Y. Honda, O. Kitao, H. Nakai, T. Vreven, J. A. Montgomery, Jr, J. E. Peralta, F. Ogliaro, M. Bearpark, J. J. Heyd, E. Brothers, K. N. Kudin, V. N. Staroverov, R. Kobayashi, J. Normand, K. Raghavachari, A. Rendell, J. C. Burant, S. S. Iyengar, J. Tomasi, M. Cossi, N. Rega, N. J. Millam, M. Klene, J. E. Knox, J. B. Cross, V. Bakken, C. Adamo, J. Jaramillo, R. Gomperts, R. E. Stratmann, O. Yazyev, A. J. Austin, R. Cammi, C. Pomelli, J. W. Ochterski, R. L. Martin, K. Morokuma, V. G. Zakrzewski, G. A. Voth, P. Salvador, J. J. Dannenberg, S. Dapprich, A. D. Daniels, Ö. Farkas, J. B. Foresman, J. V. Ortiz, J. Cioslowski and D. J. Fox, *GAUSSIAN 09 (Rev. A.1)*, Gaussian, Inc., Wallingford, CT, 2009.
84 H. S. Andrei, *PhD thesis*, University of Würzburg, Germany, 2007.
85 H. S. Andrei, N. Solca and O. Dopfer, *J. Phys. Chem. A*, 2005, **109**, 3598–3607.
86 P. J. Linstrom and W. G. Mallard, *NIST Chemistry WebBook*, NIST Standards and Technology, Gaithersburg, MD, 20899, (http://webbook.nist.gov), 2011.
87 Y. Yang, O. Kuhn, G. Santambrogio, D. J. Goebbert and K. R. Asmis, *J. Chem. Physics*, 2008, **129**, 8.
88 D. Moran, A. C. Simmonett, F. E. Leach, W. D. Allen, P. V. Schleyer and H. F. Schaefer, *J. Am. Chem. Soc.*, 2006, **128**, 9342–9343.
89 H. Horai, M. Arita, S. Kanaya, Y. Nihei, T. Ikeda, K. Suwa, Y. Ojima, K. Tanaka, S. Tanaka, K. Aoshima, Y. Oda, Y. Kakazu, M. Kusano, T. Tohge, F. Matsuda, Y. Sawada, M. Y. Hirai, H. Nakanishi, K. Ikeda, N. Akimoto, T. Maoka, H. Takahashi, T. Ara, N. Sakurai, H. Suzuki, D. Shibata, S. Neumann, T. Iida, K. Tanaka, K. Funatsu, F. Matsuura, T. Soga, R. Taguchi, K. Saito and T. Nishioka, *J. Mass Spectrom.*, 2010, **45**, 703–714 (www.massbank.jp).

90 U. Erlekam, B. J. Bythell, D. Scuderi, M. Van Stipdonk, B. Paizs and P. Maitre, *J. Am. Chem. Soc.*, 2009, **131**, 11503–11508.
91 E. P. L. Hunter and S. G. Lias, *J. Phys. Chem. Ref. Data*, 1998, **27**, 413.
92 M. P. Gaigeot, *Phys. Chem. Chem. Phys.*, 2010, **12**, 3336–3359.
93 A. A. Adesokan, G. M. Chaban, O. Dopfer and R. B. Gerber, *J. Phys. Chem. A*, 2007, **111**, 7374–7381.
94 R. Brause, H. Fricke, M. Gerhards, R. Weinkauf and K. Kleinermanns, *Chem. Phys.*, 2006, **327**, 43–53.
95 H. Mitsuda, M. Miyazaki, I. B. Nielsen, P. Carcabal, C. Dedonder, C. Jouvet, S. Ishiuchi and M. Fujii, *J. Phys. Chem. Lett.*, 2010, **1**, 1130–1133.
96 B. Kocacevic, M. Rozman, L. Klasinc, D. Srzic, Z. B. Maksic and M. Yanez, *J. Phys. Chem. A*, 2005, **109**, 8329–8335.
97 M. Majoube and G. Vergoten, *J. Mol. Spectrosc.*, 1992, **266**, 345–352.
98 A. A. El-Azhary, *Spectrochim. Acta, Part A*, 2003, **59**, 2009–2025.

